Modelling and experimental analysis of a GAX NH3-H2O gas-driven absorption heat pump.

Marcello Aprile ([1]), Rossano Scoccia, Tommaso Toppi, Marco Guerra, Mario Motta

Department of Energy, Politecnico di Milano, 20156 Milano, Italy

Abstract

The experimental analysis of a gas-driven NH_3-H_2O heat pump whose cycle approaches the GAX concept is carried out. Full load operation is investigated varying hot water temperatures and partial load operation is investigated by decreasing gas input down to 50% of the full load value. Numerical simulations bolster measurements accuracy and provide insight on the variation of cycle COP and Gas Utilization Efficiency (GUE), based on gross calorific value. A nearly constant GUE of about 1.5 is found for hot water temperatures lower than 50 °C. The GUE steadily decreases

[1] Corresponding author. Tel.: +39 02 2399 3865; fax: +39 02 2399 3868.

E-mail address: marcello.aprile@polimi.it (M. Aprile).

above 50 °C, reaching about 1.33 at 60 °C. The COP varies more smoothly, from 1.73 at 45 °C to 1.60 at 60 °C. The GUE and COP reduction at 50% of the nominal gas input is 6.8% and 6.4%, respectively. Simulations suggests that performances at partial loads can improve if active control of solution mass flow rate is implemented.

1. Introduction

With the increasing worldwide population, energy resources depletion and environmental sustainability impose new policies to promote rational use of energy and renewable energy sources. The recent "2030 framework for climate and energy policies" set new targets in terms of energy savings, share of renewables and reduction of CO_2 emissions within the EU. The new policy addresses in particular energy consumption for heating and cooling in the building sector.

A substantial contribution to energy savings and increase of the renewables share for heating can be provided by gas-driven absorption heat pumps (GAHPs), which are efficient and cost-effective alternatives to gas boilers. In a recent investigation on a new air-source ammonia-water unit developed for residential applications (Toppi et al., 2014), seasonal gas savings of 30% with respect to gas condensing boilers have been estimated for space heating in the average European climate. However, the analysis revealed that the efficient operation throughout the entire heating season is challenging for small capacity monovalent (i.e., without backup) GAHPs. A first problem is the reduced heating capacity at high thermal lifts, further penalized by frost formation occurring on the fin-tube evaporator for air-source units. Since these conditions typically occur at the design point selected for the dimensioning of the heat pump, a largely oversized heating capacity results during off-peak hours. A second but equally important problem is efficiency degradation at low partial loads, which is further penalized by cycling losses every time the actual load falls below the capacity modulation range. Since the number of operating hours at low partial loads during an entire heating season is large, the ability of the heat pump to maintain a high level of efficiency while modulating its capacity over a large modulation range becomes of crucial importance.

Although GAHPs are ready to provide environmental and economic benefits, it is desirable to further strengthen their seasonal energy performance.

In the past, ammonia-water absorption cycles have been studied extensively in order to find out the most suitable cycle configuration for residential applications, in terms of both gas efficiency and first cost (Phillips, 1990). A few cycles were identified as possible candidates, including double-effect, resorber-augmented, generator-absorber heat-exchange (GAX), double-effect regenerative, variable-effect and two-stage GAX. Among them, the GAX cycle was selected as the best choice, due to its flexibility and relatively low complexity and cost. The distinctive characteristic of the GAX cycle, firstly patented by Altenkirch and Tenckhoff (1914), is the ability to bring the rich solution in the generator above boiling point by recovering part of the absorption heat. This decreases the amount of heat externally supplied at the generator and increases the cycle COP. The internal heat recovery can be achieved because of a partial temperature overlap between generator and absorber, a condition best met at low thermal lifts. The absorber and generator sections involved in the GAX heat recovery are called, respectively, GAX absorber and GAX desorber. In the configuration proposed by Phillips, an independent hydraulic circuit connected the two, so that the liquid and the vapor streams of both absorber and desorber indirectly exchanged heat and mass in the counterflow configuration. Several studies have investigated advantages and disadvantages of the GAX cycle. As pointed out by Scharfe at al. (1986), only a small portion of the heat required by the GAX desorber can be supplied by the GAX absorber. Exergy losses in GAX heat recovery can be decreased by branching off some of the solution leaving the GAX absorber and recirculating it to the externally heated section of the generator by means of an additional solution pump (Erickson, 1991). Starting from the standard GAX cycle of Phillips, different branched GAX configurations have been simulated by Engler at al. (1997) using ABSIM software (Grossman and Zaltash, 2001). Improvements of the cycle COP over the standard GAX were reported in the range from 5 to 10%.

Garimella at al. (1996) have investigated the effect of splitting the weak absorbent, patented by Fuesting et al. (1996), in order to redirect a lower flow rate to the GAX desorber and obtain a better

temperature match between GAX absorber and desorber. Moreover, they have shown that, at high thermal lifts, a liquid heat exchanger between the weak absorbent solution and strong absorbent solution becomes more effective than the GAX absorber – desorber.

Kang and Kashiwagi (2000) have proposed a GAX configuration suited for high temperature applications (PGAX), through the branching of part of the solution after GAX absorber into a secondary water-cooled absorber and the series connection in the cooling circuit of primary and secondary water-cooled absorbers, rectifier and condenser.

An extensive review of GAX based absorption cycles, including hybrid compression-absorption, can be found e.g. in Jawahar and Saravan (2010).

A few experimental works on residential-sized GAX prototypes are also available in the literature, although these works refer mostly to the cooling operation rather than the heating one.

Experimental measurements on a breadboard basic GAX cycle prototype were performed by Erickson et al. (1996a). The cycle COP achieved about 86% of the simulated value over a wide range of thermal lifts: 0.88 in cooling at 35 °C ambient rating condition and 1.77 in heating at a lift of 48.1 °C.

In a different paper, Erickson et al. (1996b) have presented experimental analysis on a branched GAX cycle gas fired heat pump. Afterward, similar works have been carried out by Phillips (1999) and Prideman et al. (2001) on different experimental machines. The three works have shown cooling cycle COP at ARI standard rating conditions in close agreement: 0.95, 0.95 and 0.94, respectively. Prideman et al. have shown detailed simulation data in agreement with their own experimental results. The small differences were justified mainly by the lower than expected burner-generator efficiency and GAX heat recovery. It must be noticed, however, that a large difference exists in the burner-generator efficiency reported in the three independent works: 82%, 85.5% and 72.4%, respectively.

The reviewed literature provide information on the features of the GAX cycle and the possible performance improvements achievable through its modifications. However, many of the

theoretically investigated concepts do not seem to have found real application yet. Possible reasons are the high cost of the hardware and the inherent complexity of the simulated cycles. Moreover, many theoretical and experimental works focus on full load operation only, thus making difficult to evaluate if opportunities for enhancing performances at partial loads exist.

In this work, the experimental and numerical analysis of a water-source GAHP unit whose cycle approaches the GAX concept is carried out. The work aims at enhancing the knowledge about the experimental performance of the investigated GAX cycle, not only in full load operation but also at reduced loads. Moreover, this work aims to develop a validated mathematical model of the cycle, with the different purposes of providing a better understanding of the factors affecting the GAHP steady-state performance, predicting the behavior over a modulation range larger than the one currently permitted, and evaluating the possibility to preserve efficiency at low partial loads with minimal interventions on the hardware.

2. Experimental apparatus

In this section, the features of the heat pump are presented, along with the thermodynamic cycle. Moreover, the test apparatus and its measurement accuracy are briefly described. Lastly, the test activities are introduced.

2.1. Gas driven absorption heat pump

The tested absorption heat pump is a water source gas driven absorption heat pump (GAHP) manufactured by the ROBUR company, which has a nominal heating capacity of about 40 kW and is based on a Generator-Absorber-eXchange (GAX) cycle. The GAX effect, i.e. the ability to desorb part of the refrigerant by recovering the highest-grade heat released in the absorber, is implemented at the top section of the falling film solution cooled absorber (SCA), as shown in Fig. 1.

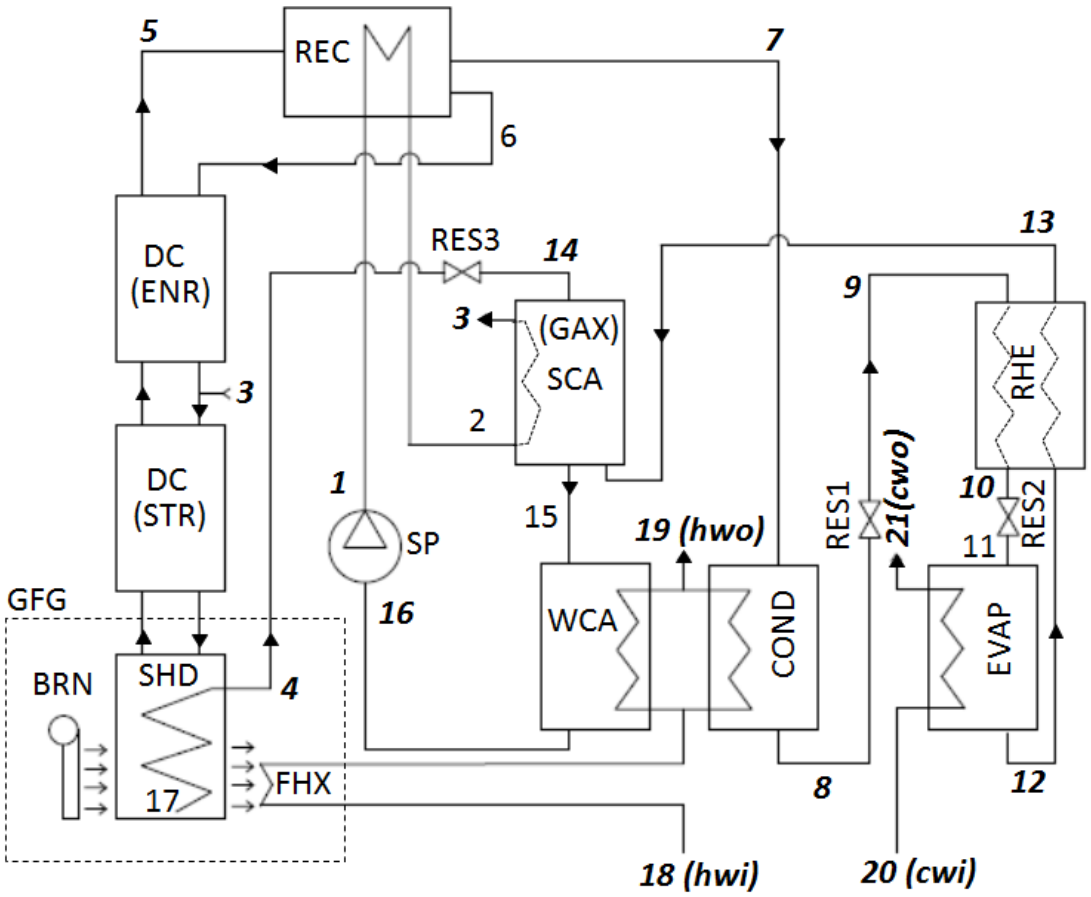

Fig. 1 – GAHP scheme.

The mixture used for the heat pump cycle is a solution of ammonia (refrigerant) in water (absorbent). In the gas-fired generator (GFG), the ammonia-water solution is externally heated using a natural gas burner (BRN) and internally heated using a heat recovery coil (SHD), through which the solution, poor in ammonia, leaves the generator. The desorbed vapor is purified through the distillation column (DC) and the rectifier (REC), where the water is further separated from the vapor through a partial condensation process. The condensate goes back to the generator while the ammonia vapor exiting the rectifier at high pressure enters the condenser (COND), where it is liquefied after being cooled down. Liquid ammonia is throttled to an intermediate pressure by means of a first restrictor (RES1), further cooled in a tube in tube heat exchanger (RHE), and lastly brought to low pressure and temperature through a second restrictor (RES2). Under these low pressure and low temperature conditions, liquid ammonia enters the evaporator (EVAP), where it

evaporates by removing heat from externally supplied water flow. The cold and low-pressure ammonia vapor exiting the evaporator flows into the RHE and then passes into the solution cooled absorber (SCA), where it is mixed with the poor solution coming from the generator and brought to a low pressure by a third restrictor (RES3). The absorption process, i.e. the dilution of ammonia vapor into the poor solution, is carried out only partially in the SCA. In order to completely absorb the vapor, the solution exiting the SCA must be further cooled down through a water cooled absorber (WCA). Once the absorption process is completed, the liquid solution rich in ammonia is pumped back to the generator at high pressure using a diaphragm solution pump (SP), operated by a hydraulic actuator. The solution is preheated both inside the coil of the REC and the SCA, where also vapor generation can occur (GAX effect), and returned to the generator where a new cycle starts. It is important to notice that the three restrictors (RES1, RES2 and RES3) are fixed. In particular, the flow rate of the solution from SHD to SCA is determined by the hydraulic characteristic of RES3, the solution properties in state 4 and the discharge pressure in state 14.

2.2. Measurement apparatus

The heat pump is equipped with thermocouples at the main cycle points, shown in bold type in Fig. 1, which are positioned on the external surface of the pipes interconnecting the cycle components, wrapped in tinfoil and fixed by means of plastic hose clamps to ensure thermal contact. A 2 cm thick layer of elastomer material provides thermal insulation. Moreover, capacitive pressures probes are used to measure REC pressure (position 7), SP input pressure (position 16) and SCA pressure (position 14). Temperatures of the external water circuits (positions 18, 19, 20, 21) are measured by immersion resistance temperature detectors (RTD), and the related flow rates by magnetic flow meters. The gas thermal input, expressed as gross calorific value, is calculated according to the Standard ISO 6976. The volumetric flow rate is measured by means of a volumetric gas flow rate counter and it is normalized based on the gas temperature and pressure measured at the meter outlet. The natural gas gross calorific value is calculated based on the composition data coming from a gas

chromatograph (model VEGA GC - MPS H10). The specific and composed uncertainties are shown in Table 1.

Table 1 – Measurement uncertainty.

	measure	**probe**	**range**	**uncertainty**
T_j	cycle point temperature	thermocouple type T	0 - 150 °C	±0.3 °C
T_{hwi}, T_{hwo}	hot water temperature	PT100	30-70 °C	±0.1 °C
ΔT_{hw}	hot water temperature difference	calculated	10-15 °C	±0.15 °C
$\dot{V}_{hw}$	how water volume flow rate	magnetic flow meter	1.5-3.0 $m^3 h^{-1}$	1.5%
Q_{hw}	heating capacity	calculated	19-45 kW	2.0%
T_{cwi}, T_{cwo}	cold water temperature	PT100	5-20 °C	±0.1 °C
ΔT_{cw}	cold water temperature difference	calculated	3-6 °C	±0.15 °C
$\dot{V}_{cw}$	cold water volume flow rate	magnetic flow meter	1.0-3.0 $m^3 h^{-1}$	1.5%
Q_{cw}	cooling capacity	calculated	6-18 kW	3.0%
Q_{GCV}	gas input	calculated	14-29 kW	2.5%
P_{16}, P_{14}	low pressure (absolute)	capacitive DP probe	3-6 bar	0.5-1.0%
P_7	high pressure (absolute)	capacitive DP probe	15-30 bar	0.2-0.4%

Notes:
The values in % are applied to the value read, not to full scale.
The uncertainty includes the probe and the measurement chain uncertainty.

2.3. Test plan

The main goal of the experimental tests is to assess the steady-state GAHP performance, in terms of cycle COP and appliance GUE. The test conditions are chosen according to the following assumptions. (1) The renewable heat source is ground water, whose temperature is constant and set at 10 °C. (2) Electricity consumption for ground water extraction is minimized through a variable speed pump that maintains a fixed temperature drop of 5 °C at the evaporator heat exchanger. Even if a slightly higher cold water outlet temperature can be achieved at partial loads with a fixed flow rate, the variable flow control strategy does not affect the thermodynamic performance of the cycle because the restrictors RES1 and RES2 are fixed, thus it is not possible to finely adjust the evaporator pressure according to the cold water outlet temperature. (3) The hot water feed temperature ranges from 45 °C to 60 °C, a range that is, on the one hand, suitable for space heating

applications at medium and high temperatures and, on the other hand, compatible with the maximum hot water temperature recommended by the manufacturer (65 °C). (4) Since the GAX cycle performance benefits from low temperatures at the hot water inlet, achievable through a careful dimensioning of the heat emission system, at full load the temperature difference between the feed and the return line in the how water loop is set to 15 °C. (5) At partial loads, setting a large hot water temperature difference is not recommended, since heat transfer at the water cooled condenser-absorber can be negatively affected by the decrease of water flow rate that is consequential to the decrease of the load. Therefore, the temperatures in the cold water loop are fixed to 10 °C inlet and 5 °C outlet for all tests. Initially, the unit is tested at full load and nominal condition (NC), i.e. hot water outlet temperature of 50 °C with a temperature difference between inlet and outlet of 15 °C, as shown in Table 2. Afterwards, the hot water feed temperature is varied to 55 °C (HT), 60 °C (VHT) and 45 °C (LT), while maintaining a fixed hot water temperature increase of 15 °C. Lastly, the performances at partial load conditions are assessed varying the gas input ratio (GIR), here defined as the ratio of the actual gas input to the gas input achieved when the speed of the combustion air blower, which is controlled by an inverter, is set to the nominal value. As shown in Table 2, GIR is varied down to 75% and 50% while maintaining the hot water feed temperature at the nominal value of 50 °C and a fixed hot water temperature difference of 10 °C.

It shall be noticed that ambient temperature has a certain influence on the full load gas input, because of combustion air density variation, and on the thermal efficiency of the generator, due to jacket losses. Therefore, it is important to limit the air temperature variations when making comparisons among different operating conditions. A value of about 5 °C is respected for all the tests.

Table 2 – Test conditions.

Test ID	T_{hwi} (°C)	T_{hwo} (°C)	T_{cwi} (°C)	T_{cwo} (°C)	GIR (%)
NC	35	50	10	5	100
HT	40	55	10	5	100
VHT	45	60	10	5	100
LT	30	45	10	5	100
75%	40	50	10	5	75
50%	40	50	10	5	50

3. Mathematical model

A mathematical model of the cycle is developed and implemented in FORTRAN code, starting from a modular simulation program specifically developed to study water-ammonia absorption cycles and already described in (Aprile et al., 2015). In order to simulate the gas fired GAX cycle, three new modules are developed and added to the existing library of components: gas fired generator, plate column, and solution cooled absorber.

3.1. Gas-fired generator

The gas-fired generator is comprised of gas burner, pool boiler with internal heat recovery and flue gas heat exchanger (see Fig. 2). Modelling the whole process is a complex task, involving, on the one hand, the calculation of the coupled radiative and convective heat transfer mechanisms occurring in the gas burner and, on the other hand, the exchange of heat and mass taking place in the pool boiler. In the latter, vapor is generated from the liquid solution under the influence of three different heat and mass transfer mechanisms: external heat input from the gas burner, heat recovery from the poor solution rising through the internal coil and partial resorption of the rising hot vapor. Moreover, the heat recoverable from condensation of the flue gas shall be determined.

The gas burner and the pool boiler with internal heat recovery are modelled by means of a simple approach. At first, the gas input ($Q_{GFG,g}$) and the combustion and thermal efficiencies of the burner (η_{cmb}, η_{th}) are defined as inputs to the model. Then, the relevant inputs and outputs are linked by

imposing the temperature pinch (ΔT_{SL}) between poor solution outlet (state point 4 in Fig. 2) and rich solution inlet (L), and the temperature difference (ΔT_{VL}) between saturated vapor outlet (V) and rich solution inlet (L). The thermal efficiency provides the heat input to the generator ($Q_{GFG,i}$), whereas the combustion efficiency provides the temperature of the flue gases at the inlet of the flue gas heat exchanger (fi). The remaining input parameters, along with integral mass, species and energy balance equations, provides the outlet states (4 and V). Pure methane and ideal combustion with 20% excess air are assumed in flue gas calculations. The condensing flue gas heat exchanger is modelled following the approach customarily used for condensing coils (Threlkeld, 1970), under the following assumptions: (1) the flue gas is modelled like an ideal gas mixture of dry gas and water vapor; (2) the properties of the dry flue gas are constant and the Lewis number is equal to one; (3) the heat exchange surface in contact with the flue gas is completely wet. The expression for the coupled heat and mass transfer is analogous to sensible heat transfer, i.e.:

$$Q_{FHX} = \varepsilon_{cf}(NTU_{wet}, C_r)\, min\,(C_f, C_{hw})\,(h_f(T_{fi}, \omega_{fi}) - h_{f,s}(T_{hwi})) \quad (1)$$

where

$$C_f = \dot{m}_{f,dry} \quad (2)$$

$$C_{hw} = \dot{m}_{hw} c_{p,hw} \left(\frac{dh_{f,s}}{dT}\bigg|_{\bar{T}_{hw}} \right)^{-1} \quad (3)$$

$$C_r = min(C_f, C_{hw}) / max(C_f, C_{hw}) \quad (4)$$

$$NTU_{wet} = (UA)_{wet} / min(C_f, C_{hw}) \quad (5)$$

The only parameter needed by the model is $(UA)_{wet}$, which can be experimentally identified.

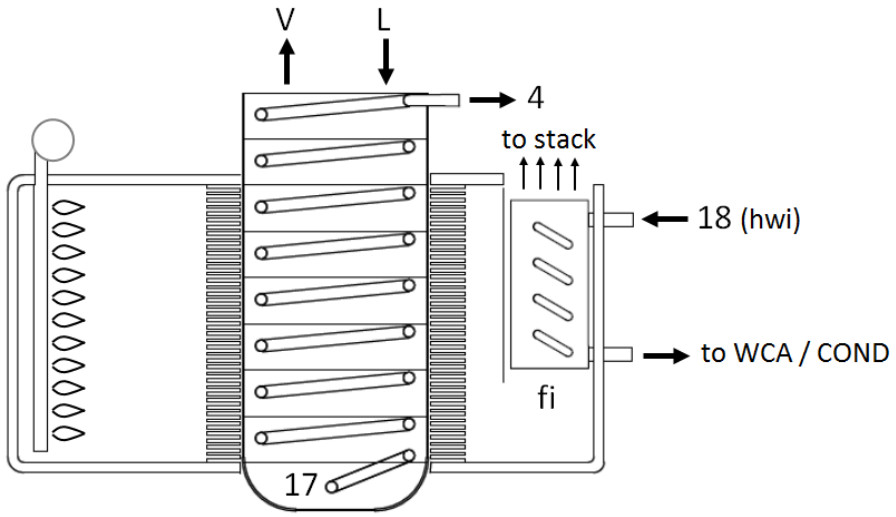

Fig. 2 – Gas-fired generator scheme.

3.2. Plate column

The plate column component is used to model the stripping and enriching sections of the distillation column. The number of ideal trays is set to one and two, respectively. The plate column is composed of a number of adiabatic ideal trays, each one having liquid inlet (i-1), liquid outlet (i-2), vapor inlet (i-3) and vapor outlet (i-4). Besides mass, species and energy balance equations, thermodynamic equilibrium of the leaving vapor (i-4) and liquid (i-2) streams is imposed, closing the system of equations for the i-tray. The component is solved iteratively with a downward pass followed by an upward pass, until convergence of temperature is achieved at each node.

3.3. Solution cooled absorber

In the solution cooled absorber (SCA), heat is exchanged between the absorbing solution (point 14 Fig. 1) and the rich solution (point 2) by means of a falling film heat exchanger. Vapor enters from the bottom and rises inside the tubes, whereas liquid solution, poor in ammonia concentration, flows down the internal surface of the tubes. On the outside surface of the tubes, heat is transferred to the rising rich solution, which first gets heated and then, in favorable operating conditions, is brought to the boiling point. The input parameters of the model are the overall heat transfer coefficient (UA),

the concentration distance from saturated liquid at the bottom (ΔX_b) and the overall pressure drop of the rich solution (ΔP_{rs}). The absorber pressure is assumed uniform (P_a). When the incoming solution is subcooled in state 14 (see Fig. 3), adiabatic mixing occurs and an equilibrium mixing point is reached (state A). The vapor mass flow rate ($\dot{m}_a$) needed to bring the incoming solution to saturated liquid state (AL) , the temperature in state A and the mass flow rate in state A are calculated as follows:

$$\dot{m}_a\, h_G(T_A, P_a, X_{AG}) \;+\; \dot{m}_{14}\, h_{14} \;=\; \dot{m}_A\, h_L(T_A, P_a, X_{AL}) \tag{5}$$

$$\dot{m}_a\, X_{AG}(T_A, P_a) \;+\; \dot{m}_{14}\, X_{14} \;=\; \dot{m}_A\, X_{AL}(T_A, P_a) \tag{6}$$

$$\dot{m}_a \;+\; \dot{m}_{14} \;=\; \dot{m}_A \tag{7}$$

The solution absorbs saturated vapor (state 13G of Fig. 3) from state A to state B while it gets cooled by the rich solution. The heat transfer rate (Q_{SCA}) determines the mass flow rate of absorbed vapor ($\dot{m}_b$) along with state B, whose concentration is set lower than the saturated liquid concentration at temperature T_{B} by a given amount (ΔX_b):

$$\dot{m}_b\, h_{13G} \;+\; \dot{m}_A\, h_A \;=\; Q_{SCA} + \; \dot{m}_B\, h_L(T_B, P_a, X_B) \tag{8}$$

$$\dot{m}_b\, X_{13G} \;+\; \dot{m}_A\, X_A \;=\; \dot{m}_B\, X_B \tag{9}$$

$$\dot{m}_b \;+\; \dot{m}_A \;=\; \dot{m}_B \tag{10}$$

$$X_B \;=\; X_L(P_a, T_B) - \Delta X_b \tag{11}$$

When the rich solution outlet state is two-phase, heat transfer rate is calculated by dividing the heat exchanger overall heat transfer coefficient and pressure drop on the single-phase (points 2-C Fig. 3) and two-phase regions (points C-3), in proportion to their respective heat transfer areas:

$$Q_{SCA} = Q_{SCA,sp} + \; Q_{GAX} \tag{12}$$

$$Q_{SCA,sp} = \varepsilon_{cf,sp} \min(C_{D-B}\,, C_{C-2})(T_D - T_2) \tag{13}$$

$$Q_{SCA,sp} = C_{D-B}(T_D - T_B) \tag{14}$$

$$Q_{SCA,sp} = C_{C-2}(T_C - T_2) \quad (15)$$

$$Q_{GAX} = \varepsilon_{cf,tp}\min(C_{A-D}\,, C_{3-C})(T_A - T_C) \quad (16)$$

$$Q_{GAX} = C_{A-D}(T_A - T_D) \quad (17)$$

$$Q_{GAX} = C_{3-C}(T_3 - T_C) \quad (18)$$

$$UA_{sp} = UA\ z \quad (19)$$

$$UA_{tp} = UA\ (1 - z) \quad (20)$$

$$P_C = P_2 - \Delta P_{rs}\ z \quad (21)$$

$$P_3 = P_2 - \Delta P_{rs} \quad (22)$$

In the above expressions, the average heat capacity rate of a stream between states i and j (C_{i-j}) is determined like the enthalpy rates difference to temperature difference ratio, i.e. $m_i|h_i - h_j|/|T_i - T_j|$. Moreover, counter flow effectiveness in each region is determined according to the related UA and heat capacity rates. Lastly, state 15 is determined as the adiabatic mixing of the streams leaving at the bottom of the absorber:

$$\dot{m}_{15} = (\dot{m}_{13G} - \dot{m}_b - \dot{m}_a) + \dot{m}_{13L} + \dot{m}_B \quad (23)$$

$$X_{15} = [(\dot{m}_{13G} - \dot{m}_b - \dot{m}_a)X_{13G} + \dot{m}_{13L}\,X_{13L} + \dot{m}_B\,X_B]/\dot{m}_{15} \quad (24)$$

$$h_{15} = [(\dot{m}_{13G} - \dot{m}_b - \dot{m}_a)h_{13G} + \dot{m}_{13L}\,h_{13L} + \dot{m}_B\,h_B]/\dot{m}_{15} \quad (25)$$

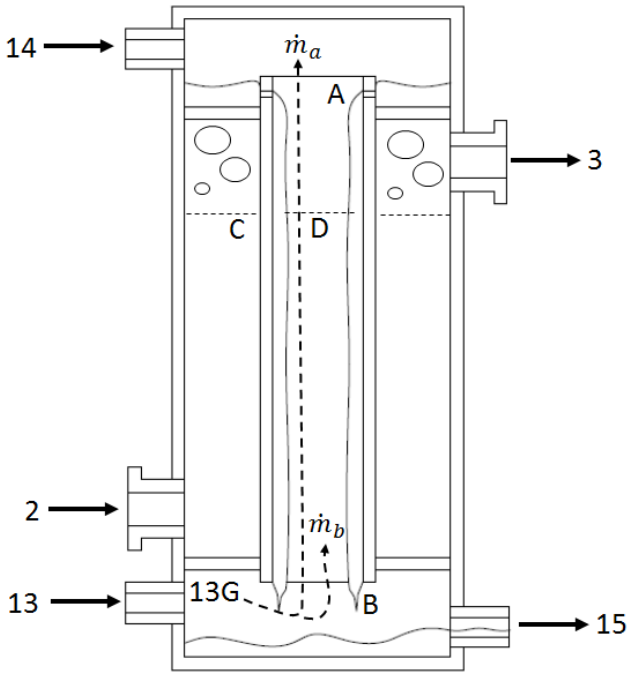

Fig. 3 – Solution cooled absorber scheme.

4. Results and analysis

The mathematical model is first calibrated against experimental data with the twofold objective to calculate state variables that are otherwise difficult to measure and to bolster the accuracy of the measurements. Based on the results provided by the calibrated mathematical model, the performances at full and partial loads are then analyzed.

4.1. Model calibration

The experimental data given in input to the model are: gas input, EVAP pressure, WCA outlet pressure, hot water inlet temperature and mass flow rate, cold water inlet and outlet temperatures. The unknown input parameters are the solution pump mass flow rate, the UA of COND, WCA, SCA, REC, RHE and FHX, the GFG parameters η_{cmb}, η_{th}, ΔT_{SL}, ΔT_{VL}, subcooling at pump inlet ($\Delta T_{sc,16}$) and at condenser outlet ($\Delta T_{sc,8}$), pressure after RES1 (P_9). For each test condition, the unknown input parameters are calibrated trying to match the following experimental data: temperature at pump outlet (T_1), temperature at SCA outlet (T_3), temperature at inlet (T_4) and outlet

(T_{14}) of solution restrictor (RES3), temperature at COND inlet (T_7) and outlet (T_8), temperature of vapor at SCA inlet (T_{13}), high pressure (P_7), temperature after RES1 (T_9), heat input at EVAP (Q_{cw}), heat output (Q_{hw}) given by the sum of Q_{FHX}, Q_{WCA} and Q_{COND}. The GFG parameters η_{cmb}, η_{th}, ΔT_{SL}, ΔT_{VL} are selected according to the output provided by a detailed model of the gas-fired generator (Aprile et al., 2016). The calibration of solution mass flow rate is performed by assuming a constant discharge factor of the solution restrictor (RES3) for the conditions in which the solution in state 14 is subcooled (NC, HT and LT, see Table 2). In such conditions, it is reasonable to assume $\dot{m} = k\sqrt{\rho \Delta p}$, where k (m^2) is a proportionality factor that characterizes the restrictor. A fixed value of 0.65 mm^2 is chosen for the proportionality factor so that the model is able to fit well the experimental data across different tests. When flashing occurs in state 14 (VHT, 75%, 50%), a lower value of the proportionality factor is identified (0.62 mm^2). For all conditions, the refrigerant temperature after EVAP (T_{12}) was set to 9.5 °C, i.e. 0.5 °C lower than T_{cwi}. Table 3 provides the summary of the calibrated input parameters. The accuracy achieved by the model after the calibration process is presented in Table 4. The general agreement with the measurements is good, except for the temperatures in positions 10 and 12. Besides the inherent difficulty in taking the measurements in these points, it shall be noticed that these temperatures have small influence on the determination of the model parameters. Lastly, the gas input and the heat duties of the different heat exchangers as provided by the model are shown in Table 5. The maximum error in the energy balance of the absorption cycle, $Q_{GFG,i}, +Q_{EVAP} - Q_{COND} - Q_{WCA}$, is less than 1%. The accuracy of the heat duties provided by the model is confirmed by the small deviations shown in Table 4 for Q_{hw} and Q_{cw} with respect to their experimental counterparts.

Table 3 – Calibrated inputs parameters.

Test ID	UA_{COND} (kW K^{-1})	UA_{WCA} (kW K^{-1})	UA_{SCA} (kW K^{-1})	UA_{REC} (kW K^{-1})	UA_{RHE} (kW K^{-1})	UA_{wet} (kg s^{-1})	η_{cmb} (%)	η_{th} (%)	ΔT_{SL} (K)	ΔT_{VL} (K)
NC	0.81	1.25	0.56	0.18	0.25	0.011	0.82	0.80	5.80	1.00
HT	0.81	1.35	0.68	0.18	0.28	0.011	0.82	0.79	7.13	1.00
VHT	0.73	1.35	0.60	0.18	0.32	0.011	0.81	0.78	7.59	1.00
LT	1.12	1.25	0.44	0.20	0.20	0.011	0.82	0.81	5.50	1.00
75%	0.70	1.13	0.48	0.11	0.15	0.009	0.83	0.81	4.30	0.80
50%	0.47	0.80	0.34	0.06	0.10	0.007	0.84	0.80	2.00	0.50

(Table 3 continuation)

$\Delta T_{sc,16}$ (K)	$\Delta T_{sc,8}$ (K)	P_9 (kPa)	$\dot{m}_1$ (kg h^{-1})
1.50	1.50	1382	142
1.50	1.00	1390	143
1.20	0.50	1262	144
2.80	8.20	1461	139
0.50	0.10	1312	118
0.10	0.05	1524	99

Table 4 – Deviations between model and experimental data.

Test ID	ΔT_1 (°C)	ΔT_3 (°C)	ΔT_4 (°C)	ΔT_5 (°C)	ΔT_7 (°C)	ΔT_8 (°C)	ΔT_9 (°C)	ΔT_{10} (°C)	ΔT_{12} (°C)	ΔT_{13} (°C)	ΔT_{14} (°C)	ΔP_7 (kPa)	ΔQ_{cw} (kW)	ΔQ_{hw} (kW)
NC	0.18	0.19	0.00	-0.08	-0.18	0.19	-0.87	-5.09	0.59	-0.53	0.55	5.29	0.19	0.29
HT	-0.16	-0.20	-0.06	-0.05	0.15	-0.14	-0.78	-4.03	1.37	0.57	0.35	3.87	-0.22	-0.10
VHT	-0.53	0.25	-0.37	-0.72	0.27	0.21	-0.90	0.29	1.84	-0.25	-0.08	5.44	-0.27	0.00
LT	0.23	-0.08	-0.3	0.16	0.76	0.28	0.13	-0.26	1.32	-0.59	0.14	1.15	0.13	-0.15
75%	-0.13	-0.07	-0.33	-0.91	0.56	-0.04	0.82	2.92	1.46	-0.40	-0.21	4.71	-0.03	0.35
50%	-0.15	0.71	-0.52	-1.68	-0.17	0.33	0.28	3.05	1.83	0.09	0.25	-0.33	-0.38	-0.39

Table 5 – Gas input and model-based heat duties.

Test ID	$Q_{GFG,g}$ (kW)	$Q_{GFG,i}$ (kW)	Q_{SHD} (kW)	Q_{FHX} (kW)	Q_{REC} (kW)	Q_{COND} (kW)	Q_{RHE} (kW)	Q_{EVAP} (kW)	Q_{SCA} (kW)	Q_{GAX} (kW)	Q_{WCA} (kW)
NC	28.50	23.05	7.94	2.78	2.60	17.65	2.14	16.32	9.59	1.15	21.85
HT	29.57	23.35	8.12	2.69	3.02	17.20	2.47	15.36	9.98	0.76	21.65
VHT	29.30	22.86	8.12	2.37	3.29	15.58	2.74	13.54	8.94	0.00	20.99
LT	29.24	23.63	8.02	3.00	2.60	18.40	1.32	17.17	9.48	1.16	22.51
75%	21.39	17.22	5.83	1.87	1.76	12.67	1.36	11.81	6.54	0.00	16.58
50%	14.25	11.40	4.01	1.43	1.05	6.99	0.69	6.76	3.70	0.00	11.26

4.2. Full load operation

The main figures of merit that characterize the behavior of the GAHP are thermal COP and Gas Utilization Efficiency based on GCV (GUE):

$$COP = (Q_{WCA} + Q_{COND}) / Q_{GFG,i} \quad (24)$$

$$GUE = (Q_{WCA} + Q_{COND} + Q_{FHX}) / Q_{GFG,g} \quad (25)$$

The effects on the GAHP performances with increasing hot water temperatures at full load are shown in Fig. 4. Both GUE and COP decrease, whereas the circulation ratio (CR), defined as the ratio of rich solution flow rate to the refrigerant flow rate, increases. The latter effect is a sign that, with higher temperatures, the difference in concentration between the rich and the poor solutions $(X_3 - X_4)$ decreases, being CR equal to $(X_7 - X_4)/(X_3 - X_4)$. With a lower concentration spread, the internal heat recovery between the desorption and the absorption processes becomes less effective. It is noticed that the GUE is about 1.5 for hot water temperatures lower than 50 °C, whereas it drops steadily for hot water temperatures above 50 °C, reaching about 1.33 at 60 °C. In comparison, the COP varies more smoothly, from 1.73 at 45 °C to 1.60 at 60 °C.

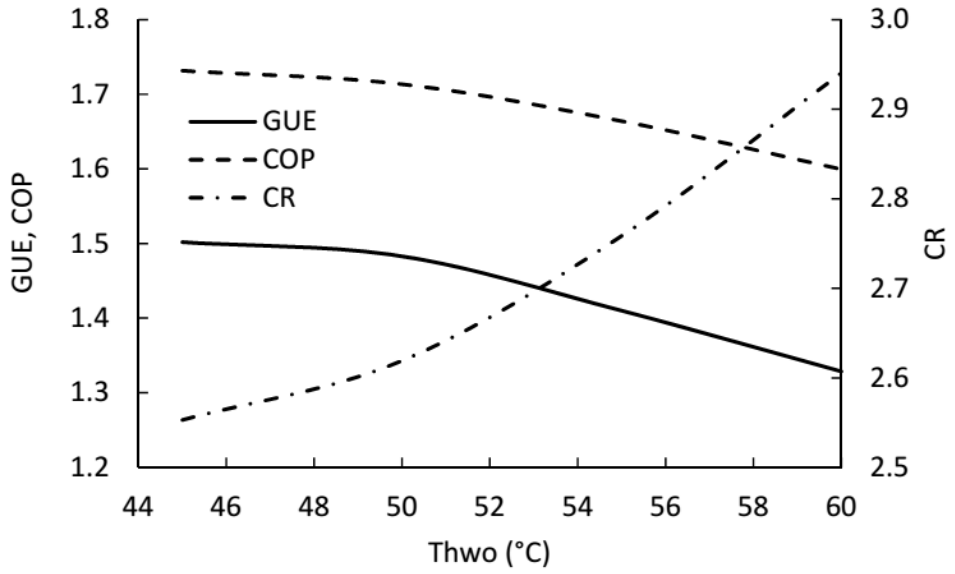

Fig. 4 – Performances at full load.

The P-T-X diagrams in Fig. (5-8) offer a clearer view of the processes occurring within the solution cycle. Since only saturated liquid states are represented in P-T-X diagrams, two points are displayed when the state is subcooled, the X point and the P point, which indicate respectively mass fraction and pressure at the temperature of the given state.

The diagrams for the LT and NC cases (Fig. 5 – 6) show similar behavior. The rich solution is highly subcooled at the pump outlet (state 1), is heated passing through REC (state 2), and achieves boiling at SCA outlet (state 3). The small reduction in liquid concentration observed between states 2 and 3 is the consequence of the GAX effect. The solution desorbs further (state 17), is cooled in the SHD (state 4) and is throttled to state 14, remaining subcooled liquid. Subcooling at this stage is beneficial if compared to saturated state: more vapor is drawn from the evaporator and the rise in temperature at the top of the SCA, consequent to adiabatic mixing (state A), increases the heat recovery potential with the rich solution. The vapor that is not drawn by the SCA mixes with the absorbing solution (state 15) and gets completely absorbed in the WCA (state 16). A main difference noticed between the LT and the NC cases concerns absorber and evaporator pressures: for the same given external temperatures at the evaporator, lower pressures are found at LT

conditions. This means that the appliance is not working in the optimal condition. In fact, an increase of the low pressures would increase the internal heat recovery through the SCA without affecting heat transfer at the evaporator, thus providing better COP. Since absorber and evaporator pressures are influenced by the initial ammonia concentration in the solution, it is likely that the initial ammonia charge is not optimized for low temperature applications.

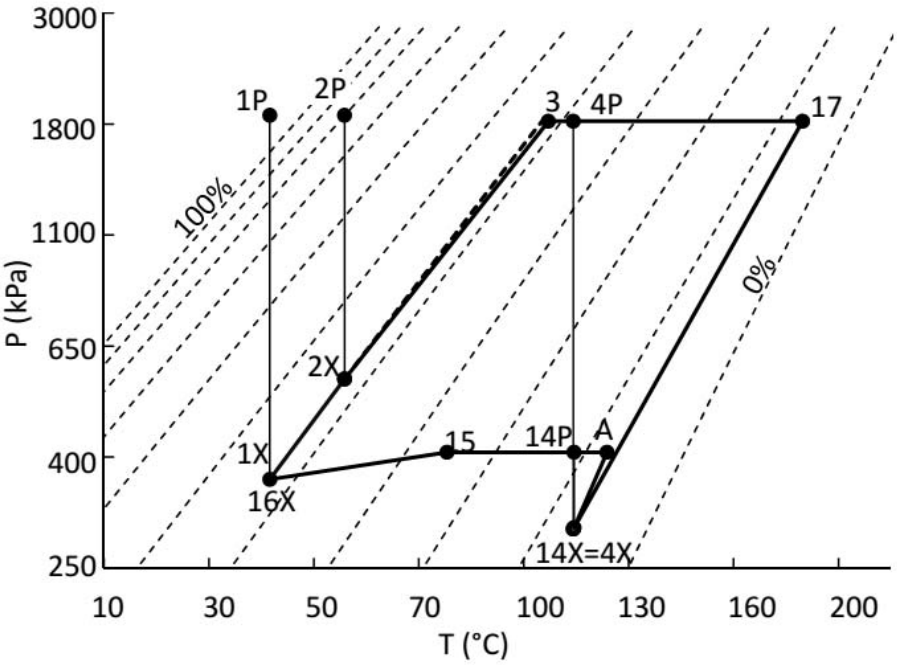

Fig. 5 – P-T-X diagram at full load (LT).

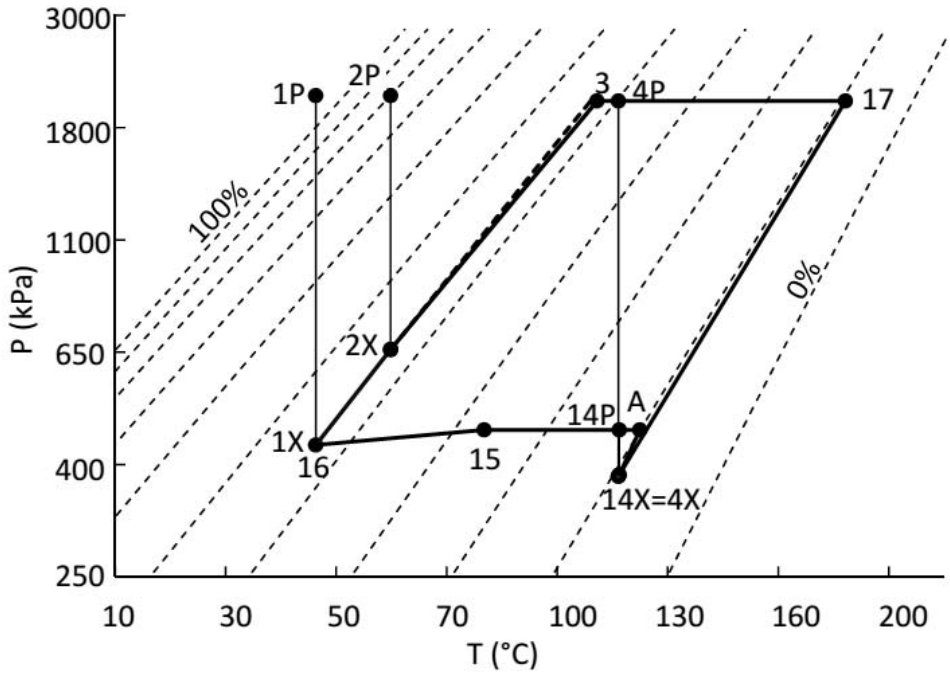

Fig. 6 – P-T-X diagram at full load (NC).

With the rise of hot water temperatures (see Fig. 7-8), remarkable changes occur in the cycle state points. The high pressure increases, while the low pressure is limited by the external temperatures at the evaporator. Due to the high pressure increase, the GAX effect first decreases (HT) and then completely vanishes (VHT). At the same time, the state at RES3 outlet (state 14) first achieves saturation (HT) and then flashing (VHT), although to a very little extent.

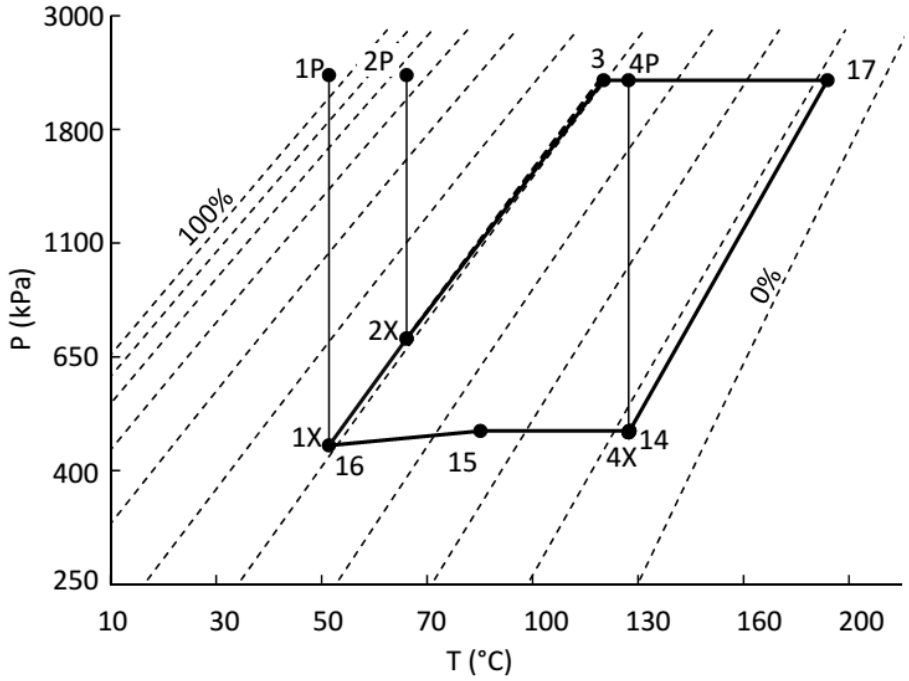

Fig. 7 – P-T-X diagram at full load (HT).

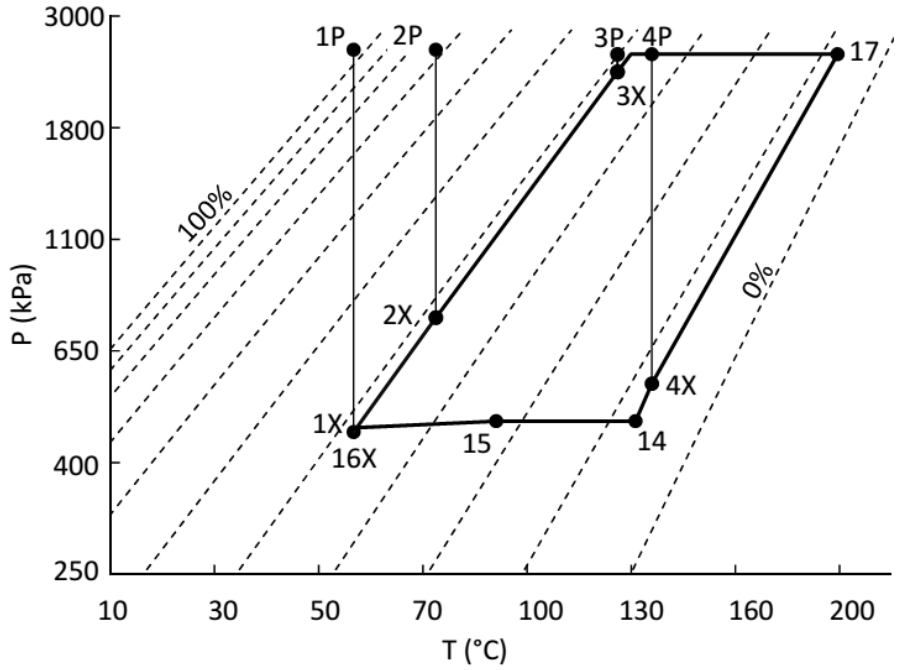

Fig. 8 – P-T-X diagram at full load (VHT).

4.3. Partial load operation

Fig. 9 shows the performances in partial load operation, by plotting the GUE, COP and CR as function of the gas input ratio (GIR). While the thermal COP immediately decreases with the reduction of gas input, the GUE initially increases and then decreases. At 50% gas input ratio, the heat duties of COND and EVAP decrease to about 40% of their full load values (see Table 5). Consequently, COP and GUE drop from 1.71 to 1.60 (-6.4%) and from 1.48 to 1.38 (-6.8%), respectively. The circulation ratio increases rapidly with the decrease of gas input, as a consequence of the enrichment of the poor solution at the bottom of the generator. This effect is better explained through the P-T-X diagrams at gas input ratio 75% (see Fig. 10) and 50% (see Fig. 11), which give an insight on the modification of the thermodynamic cycle.

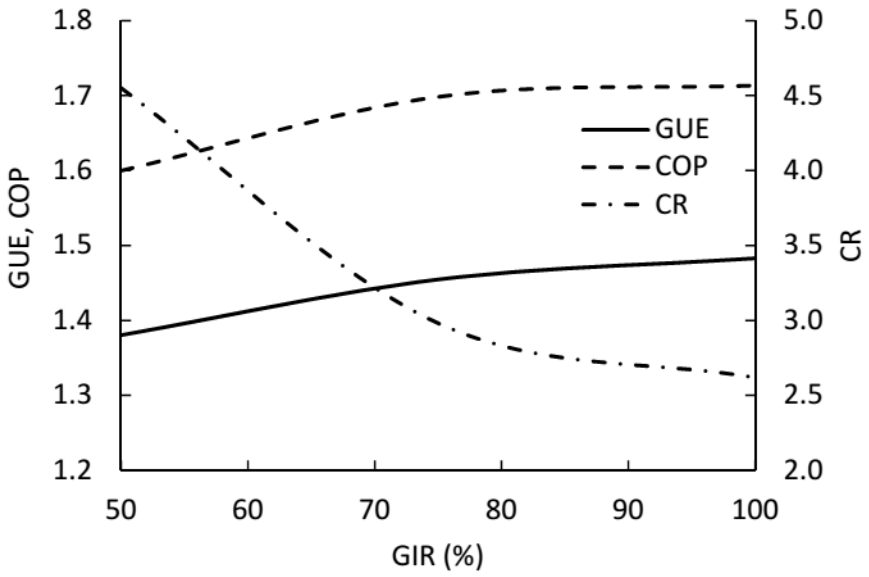

Fig. 9 – Performances at partial loads.

With the decrease of the gas input, the cooling capacity decreases, i.e., the refrigerant flow rate decreases. However, the gas input affects the flow rate of the poor solution very little, because the hydraulic characteristic of RES3 is fixed and the pressures in states 4 and 3 are strongly influenced

by the hot water outlet temperature and the cold water outlet temperature, which are held constant. Consequently, the decrease of the rich solution flow rate is lower than proportional with respect to gas input. This means that, at parity of other conditions, the highest temperature in the cycle (state 17) decreases and the concentration in the solution leaving the generator increases. With a reduced spread of concentration between the rich and the poor solutions, the heat recovery potential between absorption and desorption processes is strongly penalized. Flashing occurs after the solution restrictor (state 14), with a sharp drop in temperature that dissipates a fraction of the heat recovery potential. This fact explains why the GAX effect vanishes at partial loads (see Table 5). At the same time, mixing of the subcooled rich solution (state 3) with the vapor rising through the DC causes a rapid temperature increase that limits the heat recovery potential in the SHD, i.e., increases the temperature approach between states 4 and 3. This effect is not yet evident at 75% gas input ratio (see Fig. 10). In fact, flashing after the restrictor increases the resistance to flow along the solution path from generator to SCA, causing a sort of self-adjusting mechanism of the solution flow rate. However, the penalizing effect becomes evident at 50% gas input ratio, which is characterized by a marked temperature difference between states 4 and 14, along with the large distance of state 3 from the rich solution boiling point (see Fig. 11).

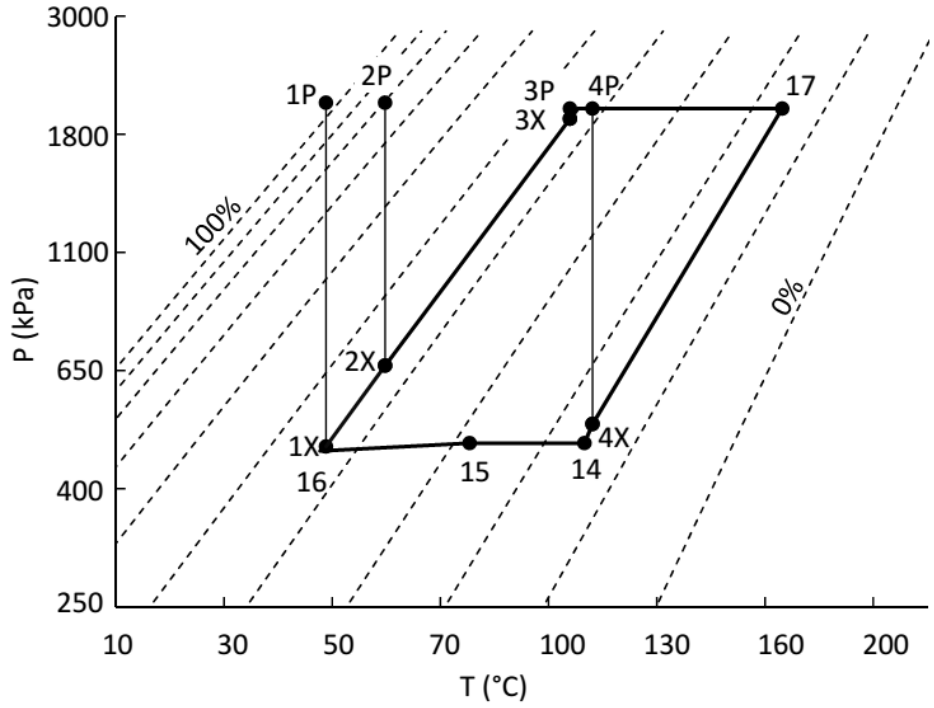

Fig. 10 – P-T-X diagram at partial load (75%).

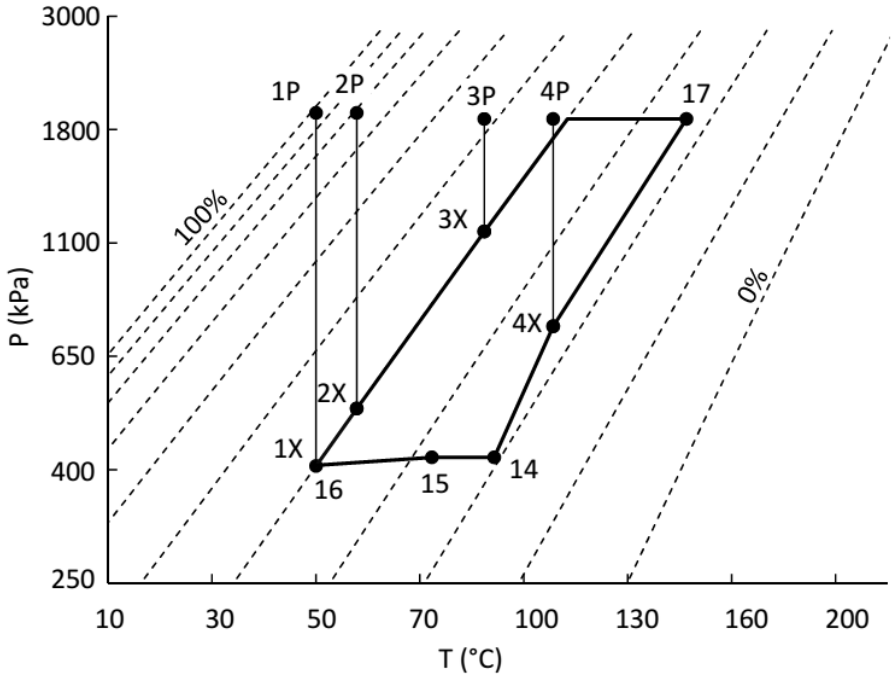

Fig. 11 – P-T-X diagram at partial load (50%).

From the previous analysis, it is concluded that the circulation ratio tends to become too large at low gas input ratios. This effect is further explored for gas input ratios below 50% by means of numerical simulations. As shown in Table 3, the UA-values vary with the load (i.e., test conditions

NC, 75% and 50%), because of the variations of the related flow rates that affect UA-values not only through the heat transfer coefficients but also through the wettability of the exchange surfaces and the internal flows distribution. Therefore, it is important to consider the variation of the UA-values also at gas input ratios below 50%. Based on the results of the calibration, an extrapolation of the UA-values of main heat exchangers (SCA, WCA, COND, RHE, REC, FHX) is carried out for gas input ratios 20% and 35% (see Table 6). The flow rates used for the extrapolation are the inlet solution flow rate for the two absorbers, the refrigerant flow rate for COND, RHE and REC, and the flue gas flow rate for FHX.

Table 6 – UA-values at partial loads.

GIR	UA_{COND} (kW K^{-1})	UA_{WCA} (kW K^{-1})	UA_{SCA} (kW K^{-1})	UA_{REC} (kW K^{-1})	UA_{RHE} (kW K^{-1})	UA_{wet} (kg s^{-1})
75%	0.70	1.13	0.48	0.110	0.15	0.009
50%	0.47	0.80	0.34	0.060	0.10	0.007
35%	0.36	0.62	0.26	0.035	0.07	0.005
20%	0.22	0.38	0.15	0.018	0.05	0.003

The performances predicted by the model in this extended modulation range are shown in Fig. 12 (square markers). A sharp drop of the efficiency is observed below 50 %, along with a sharp increase of the solution circulation ratio. In particular, GUE drops from 1.48 at full load to 1.11 at 20% gas input ratio, i.e. a 25% drop.

The detrimental effect on GUE due to the increasing circulation ratio suggests that a possible way to improve performances at low partial loads might consist in actively reducing the solution flow rate. Fine-tuning of solution flow rate can be achieved by changing the hydraulic characteristic of the restrictor valve RES3. For simplicity, only the effect of an alternate ‘low flow’ restrictor valve, to be used in the modulation range between 20% and 75%, is analyzed. With a different range of solution and refrigerant flow rates, a new extrapolation of the UA-values is needed (see Table 7).

Table 7 – UA-values at partial loads, low flow restrictor.

GIR	UA_{COND} (kW K^{-1})	UA_{WCA} (kW K^{-1})	UA_{SCA} (kW K^{-1})	UA_{REC} (kW K^{-1})	UA_{RHE} (kW K^{-1})	UA_{wet} (kg s^{-1})
75%	0.7	0.92	0.39	0.110	0.15	0.009
50%	0.48	0.65	0.27	0.061	0.10	0.007
35%	0.38	0.45	0.18	0.037	0.07	0.005
20%	0.25	0.20	0.08	0.020	0.06	0.003

As shown in Fig. 12 (round markers), the increase of the circulation ratio with the decrease of gas input is much less pronounced, ranging from 2.5 to 7.5. Therefore, the model predicts substantial improvements of the partial load efficiency. With a low flow restrictor valve, the GUE at 20% gas input ratio increases from 1.11 to 1.27. With respect to the full load value, this represents only a 14% drop.

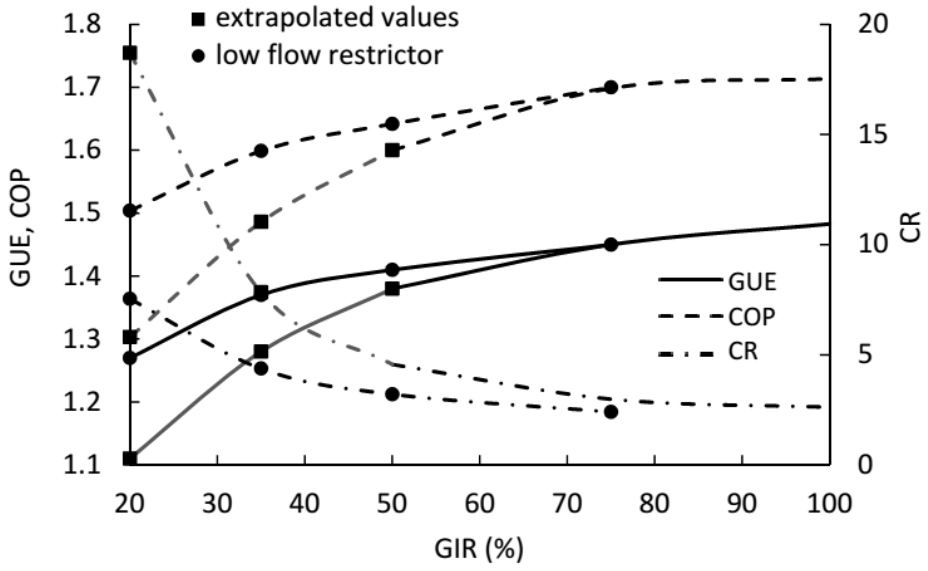

Fig. 12 – Extended modulation range.

5. Conclusions

The performances of a water-source gas-driven NH3-H2O absorption heat pump, whose cycle approaches the GAX concept, have been numerically and experimentally investigated. The analysis has focused on the influence of hot water temperature and gas input on both thermal COP and Gas

Utilization Efficiency. In parallel to the experimental activities, a mathematical model of the unit was developed and calibrated according to the experimental data, in order to derive unknown concentrations and mass flow rates in the cycle. The model provided insight of the factors affecting the performance at the different operating conditions.

At full load and with increasing hot water temperatures, both GUE and COP decreased due to the lowering of the concentration spread and the resulting loss in effectiveness of the internal heat recovery between the desorption and the absorption processes, an inherent problem of the investigated cycle. The model has shown that, with cold water inlet temperature of 10 °C, the GAX effect vanishes with hot water outlet temperature above 50 °C. Moreover, the nearly flat curves of GUE and COP for hot water temperatures below 50 °C are likely to be associated to the initial charge of ammonia, which was optimized for high temperature applications.

With decreasing gas input from 100% to 50% of the nominal value, COP and GUE dropped by 6.4% and 6.8%, respectively. An extrapolation of the efficiency values at gas input ratio below 50% has been made through the calibrated mathematical model of the cycle. The predicted GUE at 20% gas input ratio dropped by 25%, with respect to the full load GUE. The analysis suggested that margin for performance improvements could exist by actively controlling the solution flow rate on the solution path from generator to SCA. The model predicted that, by using a low flow restrictor valve, the modulation range could be extended down to 20% gas input ratio with a drop in efficiency of only 14% with respect to the full load value.

REFERENCES

Altenkirch, E., Tenckhoff, B., 1914. Absorptionskaeltemaschine zur kontinuierlichen erzeugung von kaelte und waerme oder acuh von arbiet. German Patent 278076.

Aprile, M., Toppi, T., Guerra, M., Motta, M., 2015. Experimental and numerical analysis of an air-cooled double-lift NH_3-H_2O absorption refrigeration system, Int. J. Refrigeration 50, 57-68.

Aprile, M., Toppi, T., Guerra, M., Motta, M., 2016. Analysis of a gas-fired NH_3-H_2O generator with cross-flow gas burner, Applied Thermal Engineering 93, 1216–1227.

Engler, M., Grossman, G., Hellmann, H.-M., 1997. Comparative simulation and investigation of ammonia-water: absorption cycles for heat pump applications, Int J. Refrigeration 20, 504-516.

Erickson, D. C., 1991. Branched GAX absorption vapor compressor. US Patent 5,024,063

Erickson, D.C., Papar, R. A., Anand, G., 1996a. Basic GAX cycle prototype results, International Ab-sorption heat pump conference 1996, Montreal, Quebec, Canada, 717-724.

Erickson, D.C., Papar R. A., Anand, G., 1996b. Branched GAX cycle gas fired heat pump, Intersociety Energy Conversion Engineering Conference, 2, 1078-1083.

Fuesting, D.A., Stephan W. E., Merrick, R. H., 1996. Generator absorber heat exchanger for an ammonia/water absorption refrigeration system, United States Patent 5,490,393.

Garimella, S., Christensen, R. N., Lacy, D., 1996. Performance evaluation of a generator-absorber heat-exchange heat pump, Applied Thermal Engineering 16, 591-604.

Grossman, G., Zaltash, A., 2001. ABSIM — modular simulation of advanced absorption systems. Int. J. Refrigeration 24, 531-543.

ISO 6976, 1995. Natural gas - calculation of calorific values, density, relative density and wobbe index from composition.

Jawahar, C.P., Saravanan, R., 2010. Generator absorber heat exchange based absorption cycle – A review, Renewable and Sustainable Energy Reviews 14, 2372-2382.

Kang, Y. T., Kashiwagi, T., 2000. An environmentally friendly GAX cycle for panel heating: PGAX cycle, Int. J. Refrigeration 23, 378-387.

Phillips, B. A., 1990. Development of a high-efficiency, gas-fired, absorption heat pump for residential and small-commercial applications. Phase I Final Report - Analysis of advanced Cycles and selection of the preferred cycle, Final Report on Oak Ridge National Laboratory Subcontract 86X-24610C.

Phillips, B. A., 1999. Advances on Ammonia-Water Heat Pumps for Residential Use, International Sorption Heat Pump Conference, Germany.

Prideman, D. K., Garrabrant, M. A., Mathias, J. A., Stout, R. E., Christensen, R., N., 2001. Performance of a residential-sized GAX absorption chiller, Transactions of the ASME 123, 236-241.

Sharfe, J., Ziegler, F., Radermacher, R., 1986. Analysis of advantages and limitations of absorber-generator heat exchange, Int. J. Refrigeration 9, 326-333.

Threlkeld, J.L., 1970. Thermal Environmental Engineering, Prentice-Hall, New York, Second Edition.

Toppi, T., Aprile, M., Motta M., Bongs, C., 2014. Seasonal performance calculation and transient simulation of a newly developed 18 kW air-source water-ammonia gas heat pump for residential applications, IEA Heat Pump Conference 2014, Montreal, Canada, Paper O.3.6.2.

Nomenclature

C	heat capacity rate, W K^{-1}
c_p	specific heat capacity, J kg^{-1} K^{-1}
CR	circulation ratio = m_1/m_7, -
h	enthalpy, J kg^{-1}
k	proportionality factor of the restrictor, m^2
$\dot{m}$	mass flow rate, kg s^{-1}
NTU	number of transfer units
P	pressure, Pa
Q	heat transfer rate, W
T	temperature, K
UA	overall heat transfer coefficient, W K^{-1}
$\dot{V}$	volumetric flow rate, m^3 s^{-1}
X	ammonia mass fraction, kg kg^{-1}
z	fraction of exchange area in contact with single phase fluid

Greek symbols

Δ	difference
ε_{cf}	effectiveness of counter-flow heat exchanger
η_{cmb}	combustion efficiency
η_{th}	thermal efficiency
ω	humidity ratio of flue gas, kg kg^{-1}
ρ	density, kg m^{-3}

Subscripts

cw	cold water
cwi	cold water inlet
cwo	cold water outlet
dry	dry gas
ex	exchanged
f	flue gas
FL	full load
G	gas phase
GCV	gross calorific value
GFG_G	gas input to generator
GFG_i	heat input to generator
hw	hot water
hwi	hot water inlet
hwo	hot water outlet
L	liquid phase
rs	rich solution
s	saturated
sc	subcooling
SL	solution outlet – liquid inlet
sp	single phase
tp	two phase
VL	vapor outlet – liquid inlet
wet	condensing mode

Abbreviations

BRN burner

COND condenser

COP thermal coefficient of performance

DC distillation column

ENR enriching section

EVAP evaporator

FHX flue gas heat exchanger

GAHP gas driven absorption heat pump

GAX generator absorber heat exchange

GIR gas input ratio

GFG gas fired generator

GUE gas utilization efficiency

SP solution pump

REC rectifier

RES restrictor

RHE refrigerant heat exchanger

SCA solution cooled absorber

SHD solution heated desorber

STR stripping section

WCA water cooled absorber